A&A 559, A49 (2013)
DOI: 10.1051/0004-6361/201321453

Astronomy & Astrophysics

CO_2 formation on interstellar dust grains: a detailed study of the barrier of the CO + O channel

M. Minissale[1], E. Congiu[1], G. Manicò[2], V. Pirronello[2], and F. Dulieu[1]

[1] LERMA, UMR8112 du CNRS, de l'Observatoire de Paris et de l'Université de Cergy Pontoise, 5 mail Gay Lussac, 95000 Cergy Pontoise Cedex, France
e-mail: marco.minissale@obspm.fr
[2] Dipartimento di Fisica ed Astronomia, Universitá degli Studi di Catania, via Santa Sofia 64, 95123 Catania, Italy

Received 12 March 2013 / Accepted 5 September 2013

ABSTRACT

Context. The formation of carbon dioxide in quiescent regions of molecular clouds has not yet been fully understood, even though CO_2 is one of the most abundant species in interstellar ices.
Aims. CO_2 formation is studied via oxidation of CO molecules on cold surfaces under conditions close to those encountered in quiescent molecular clouds.
Methods. Carbon monoxide and oxygen atoms are codeposited using two differentially pumped beam lines on two different surfaces (amorphous water ice or oxydized graphite) held at given temperatures between 10 and 60 K. The products are probed via mass spectroscopy by using the temperature-programmed desorption technique.
Results. We show that the reaction CO + O can form carbon dioxide in solid phase with an efficiency that depends on the temperature of the surface. The activation barrier for the reaction, based on modelling results, is estimated to be in the range of 780−475 K/k_b. Our model also allows us to distinguish the mechanisms (Eley Rideal or Langmuir-Hinshelwood) at play in different temperature regimes. Our results suggest that competition between CO_2 formation via CO + O and other surface reactions of O is a key factor in the yields of CO_2 obtained experimentally.
Conclusions. CO_2 can be formed by the CO + O reaction on cold surfaces via processes that mimic carbon dioxide formation in the interstellar medium. Astrophysically, the presence of CO_2 in quiescent molecular clouds could be explained by the reaction CO + O occurring on interstellar dust grains.

Key words. publications, bibliography – astrochemistry – atomic processes – ISM: abundances – ISM: atoms – ISM: molecules

1. Introduction

Carbon dioxide has already been detected in the interstellar medium (ISM) by d'Hendecourt & Jourdain de Muizon already few decades ago (1989). It represents one of the most common and abundant types of ices, and many astronomical observations (by the Infrared Space Observatory and the *Spitzer* Space Telescope) confirm the presence of CO_2 in different environments, such as Galactic-centre sources (de Graauw et al. 1996), massive protostars (Gerakines et al. 1999; Gibb et al. 2004), low-mass young stellar objects (Nummelin et al. 2001; Aikawa et al. 2012), brown dwarfs (Tsuji et al. 2011) background stars (Knez et al. 2005), in other galaxies (Shimonishi et al. 2010; Oliveira et al. 2011), and in comets (Ootsubo et al. 2010). CO_2 is predicted to have low abundance in the gas phase ($N_{CO_2}/N_{H_2} = 6.3\times10^{-11}$; Herbst & Leung 1986), and this is confirmed by observations (van Dishoeck et al. 1996). Low abundances in gas phase, together with its observed high abundances in the solid phase, cannot be explained exclusively by formation via gas-phase schemes (Hasegawa et al. 1992), therefore surface reactions are evoked to justify a high abundance of carbon dioxide ices.

Extensive experimental studies have been carried out to study formation routes of CO_2 formation in solid-phase. Energetic routes, such as irradiation of CO ices (pure or mixed with H_2O) with photons, charged particles or electrons, have been investigated by Gerakines et al. (1996), Palumbo et al. (1998), Jamieson et al. (2006), Ioppolo et al. (2009), and Laffon et al. (2010), and have shown an efficient formation of carbon dioxide. Whittet et al. (1998), however, provided the evidence of efficient CO_2 formation in quiescent dark clouds towards the line of sight Elias 16. This suggests that the presence of CO_2 in grain mantles can also be explained through chemical pathways occurring without the addition of energy and where the radicals are thermalized with the surface. Two of these pathways are

1. $CO + OH \rightarrow CO_2 + H$
2. $CO + O \rightarrow CO_2$.

In recent experimental studies it has clearly been shown that reaction 1 leads to CO_2 formation, although no consistent results were obtained concerning the activation barrier: little or barrierless in Oba et al. (2011) and "high" (400 K) in Noble et al. (2011). Reaction 2 has been studied theoretically (Talbi et al. 2006; Goumans et al. 2008), and those studies suggest there is a high activation barrier (2500−3000 K). The first successful laboratory investigation of the formation of CO_2 by non-energetic processes was performed by Roser et al. (2001), who studied the surface reaction of CO and O atoms. In a first set of experiments they co-deposited the two species at 5K and performed a temperature-programmed desorption (TPD). Probably due to the low sensitivity of the quadrupole mass spectrometer they were using at that time, they did not detect any CO_2 formation. To prove the formation of carbon dioxide through such a pathway and to give a first estimate of the barrier for such a reaction they subsequently devised an experiment in which the co-deposited layer of CO and O atoms was covered by a layer of porous water ice. The TPD performed in such conditions allowed the formation of CO_2 to be detected thanks to the reaction of CO and

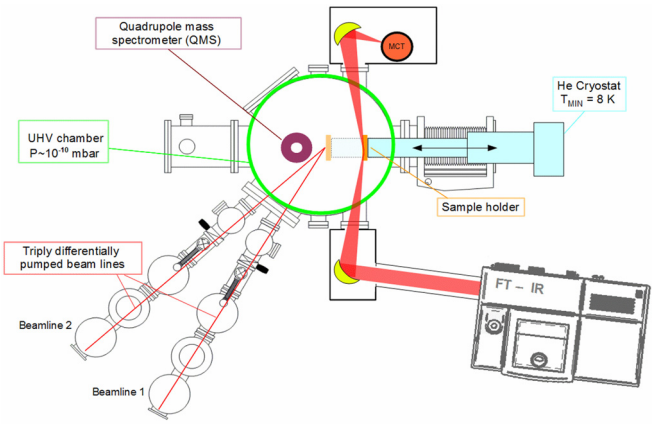

Fig. 1. Schematic top-view of the FORMOLISM setup and the FT-RAIRS facility.

O migrating in the interconnected pores of the amorphous ice. Under the hypothesis that the mobility of species stemmed from thermally activated processes, a reaction barrier of 290 K was obtained that explained the formation of carbon dioxide even in quiescent clouds[1]. Raut & Baragiola (2011) confirmed the formation of CO_2 by Roser et al. (2011). They performed experiments showing the formation of small amounts CO_2 during co-deposition of CO and cooled O and O_2 at 20 K, although they did not provide any activation barrier for reaction 2. Here we present further experimental studies of reaction 2. CO_2 production on cold surfaces (10–40 K) was investigated by concurrent exposures of CO molecules and O atoms. The CO + O reaction is studied in a submonolayer regime on two different substrates: amorphous solid water (ASW) ice and oxidized graphite. As previously found in Raut & Baragiola (2011), CO_2 formation is in competition with O_2 and O_3 formation via the O + O and O_2 + O reaction routes. We also determined an activation energy of the CO + O reaction and the physical chemical mechanisms occurring on the surface by developing a kinetic model.

2. Experiments

The experiments were performed with the FORMOLISM (FORmation of MOLecules in the InterStellar Medium) set-up (Fig. 1), which is described elsewhere (Amiaud et al. 2006; Congiu et al. 2012). The set-up is dedicated to investigating physical chemical reactions on surfaces of astrophysical interest, under conditions roughly similar to those encountered in the ISM. Experiments take place in an ultra-high vacuum chamber (base pressure 10^{-10}–10^{-11} mbar) containing a graphitic sample surface (0.9 cm in diameter), operating at temperatures between 10 and 400 K. The temperature is controlled by a calibrated silicon-diode sensor and a thermocouple (AuFe/Chromel K-type) clamped on the sample holder. The system is equipped with a quadrupole mass spectrometer (QMS), which is used for temperature-programmed desorption (TPD) experiments. ASW ice is grown in situ on the graphite sample. The H_2O vapour is obtained from deionized water previously purified by several freeze-pump-thaw cycles carried out in a vacuum. H_2O molecules are deposited on the surface maintained at 110 K through a leak valve equipped with a micro channel doser positioned at 3.5 cm in front of the cold surface during the water ice deposition phase. The ^{13}CO molecules and O atoms are sent simultaneously (co-deposition) on the surface via two triply differentially pumped beam lines. We used ^{13}CO instead of ^{12}CO to increase the signal-to-noise ratio of the mass signal of the CO reactant and the final CO_2 product. Hereafter we refer to ^{13}CO as CO. The O atoms are produced by dissociation of O_2 molecules. The two beam lines are equipped with microwave dissociation sources (surfatron cavities delivering 200 W at 2.45 GHz) that can generate atoms by breaking molecular internal bonds. With the microwave source turned on, the dissociation efficiency of O_2 was $\tau = 73 \pm 5\%$ at the time of the experiments performed on ASW and $61 \pm 7\%$ when we perfomed the experiments on graphite[2]. Atoms and undissociated molecules are cooled and instantaneously thermalized upon surface impact with the walls of the quartz tube.

We have calibrated the molecular beam as described in Amiaud et al. (2007) and Noble et al. (2012) and found that the first monolayer (1 ML = 10^{15} molecules cm^{-2}) of both ^{13}CO and O_2 was reached after an exposure time of about six minutes, which therefore gives a flux $\phi_{O_2off,CO} = (3.0 \pm 0.3) \times 10^{12}$ molecules cm^{-2} s^{-1}. Once the O_2 discharge is turned on, the O-atom flux is $\phi_O = 2\tau\,\phi_{O_2off} = 5.4 \times 10^{12}$ atoms cm^{-2} s^{-1} and the O_2 flux $\phi_{O_2on} = (1-\tau)\,\phi_{O_2off} = 10^{12}$ molecules cm^{-2} s^{-1}. In addition, we determined that the beam did not contain O or O_2 in an excited state by tuning the ionizing electron energy inside the QMS head as described in Congiu et al. (2009).

CO_2 formation was investigated on two different surfaces, ASW and oxidized graphite. Fixed doses of O ($+O_2$), 0.5 ML, and CO, 0.5 ML, were deposited on the surface held at a given constant temperature. After each deposition, the surface was heated with a linear temperature ramp of 10 K/min until the adsorbate had fully desorbed from the surface (around 90–95 K). The surface was then cooled again so that a new deposition could begin at a different temperature. For both substrates (ASW ice and graphite), we used eight surface temperatures (10, 20, 30, 35, 40, 45, 50, 60 K).

We also performed an experiment to check the CO reactivity with O_2 and O_3 to form CO_2. For this purpose, we performed two sets of TPD experiments. First, the CO + O_2 reaction was checked with a set of experiments consisting of three different depositions – each one followed by TPD – with the surface temperature held at 10 K: 2 ML of CO + 2 ML of O_2 and the co-deposition of 2 ML CO and O_2. The CO + O_3 reaction was studied through a similar set of experiments except that we had previously produced ozone via the O + O_2 reaction occurring on the surface, eliminated the residual O_2 by heating to 50 K, and only then, deposited CO at 10 K.

3. Experimental results

From an energetic point of view, oxidation of CO to form carbon dioxide may proceed by the following reactions:

1a. $CO + O \rightarrow CO_2$ ($-\Delta H = 532$ kJ/mol)
2a. $CO + O_2 \rightarrow CO_2 + O$ ($-\Delta H = 33$ kJ/mol)
3a. $CO + O_3 \rightarrow CO_2 + O_2$ ($-\Delta H = 425$ kJ/mol)[3].

To disentangle which of these reactions are effectively able to produce CO_2 on cold surfaces, we have to be sure that CO_2 is really formed on the surface and that it is not present as

[1] Nevertheless we notice that the experimental conditions were not completely consistent with physical chemical conditions of quiescent molecular clouds.

[2] τ represents the percentage of O_2 molecules dissociated, which also defines the O/O_2 ratio in the beamline; e.g., every 10 O_2 molecules, if τ is 0.7, we will have 14 O atoms and 3 O_2 molecules.

[3] NIST Chemistry WebBook.

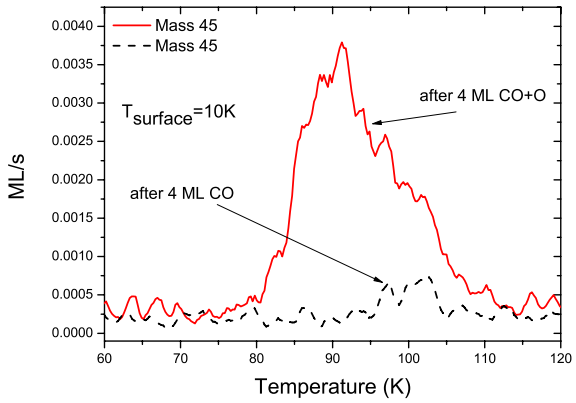

Fig. 2. TPD curves of mass 45 ($^{13}CO_2$) between 60 and 120 K after 4 ML of ^{13}CO exposure (dotted curve), and after 4 ML of $^{13}CO + O$ (solid line) on graphite held at 10 K.

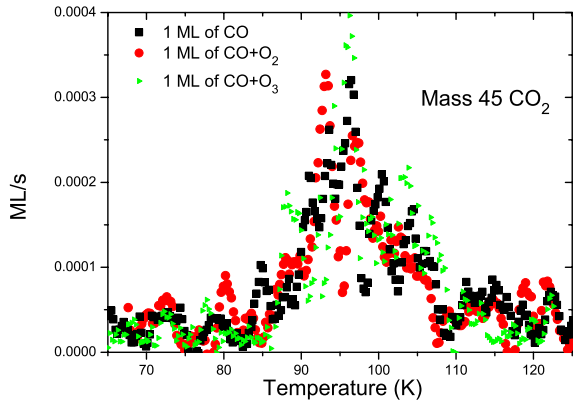

Fig. 3. TPD curves of mass 45 ($^{13}CO_2$) between 65 and 125 K after deposition of 1 ML of ^{13}CO (squares), $^{13}CO + O_2$ (circles) and $^{13}CO + O_3$ (triangles) on graphite held at 10 K.

an impurity in the CO bottle. To check this possibility, we have performed further experiments. In Fig. 2 we show one of these tests where we checked the CO_2 presence on the graphite surface – held at 10 K – after an exposure of 4 ML of CO and after 4 ML of CO + O. The difference between the two TPDs is evident, and comparing the two CO_2 signals we find CO_2(CO dep)/CO_2(CO + O dep) ~ 8%, which confirms that the majority of the CO_2 detected is formed through surface reactions.

Roser et al. (2001) and Raut & Baragiola (2011) have already studied reaction 1a, showing that this reaction can produce carbon dioxide without the intervention of energetic processes. As for reaction 2a, Mallard et al. (1994) suggested a very high activation energy barrier (~24 000 K), while reaction 3a, to the best of our knowledge, has not been studied yet. In our experimental set-up, the oxygen atom beam is produced through dissociation of O_2 molecules with a dissociation fraction which never exceeds 80%. This means that we always have an O_2 "pollution". Moreover, when O atoms arrive on the surface, they efficiently recombine to form O_2 and O_3 (Minissale et al. 2013).

For these reasons, it is not possible to study reaction 1a without knowing how (and if) reaction 2a and 3a work. Figure 3 shows three TPD spectra of mass 45 after deposition on oxidized graphite held at 10 K of 1 ML CO, co-deposition of 1 ML CO + O_2, and 1 ML CO + O_3. The three TPD curves and integrated areas of the curves are very similar and this suggests that the CO + O_2 reaction does not occur or that at least it is

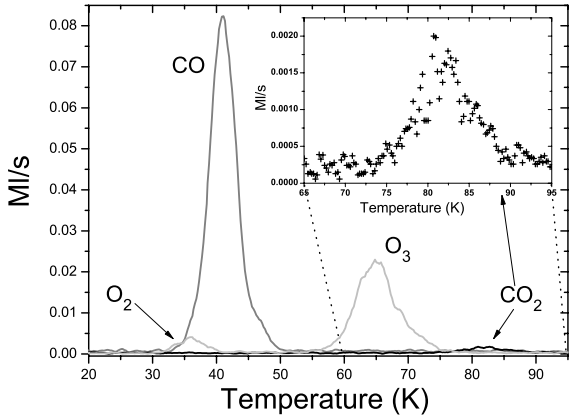

Fig. 4. TPD curves at mass 29, 32, and 45 after irradiation of 0.5 ML of $^{13}CO + O$ on ASW ice held at 20 K. Four peaks are visible. The first peak between 28 K and 42 K is due to O_2 desorption, the second one between 32 and 55 K is due to ^{13}CO desorption. The third peak between 55 K and 75 K represents O_3 desorption, while the high-temperature peak is the desorption of $^{13}CO_2$ (75–95 K).

very inefficient at producing CO_2 in accord with Mallard et al. (1994). We have another indication of the CO + O_2 inefficiency by comparing the area of the CO peak with and without O_2. In the two cases we do not detect any measurable variations of the CO yield. We get to the same conclusion as far as the CO + O_3 reaction is concerned. No difference can be appreciated in the comparison between the peak area of CO, of background CO_2 and of O_3. This indicates that CO + O_3 is not a fast reaction to produce CO_2 either.

In Fig. 4 we show the TPD traces resulting from irradiating ASW ice held at 20 K with 0.5 ML of CO + O (i.e., 0.5 ML CO, 0.15 ML O_2, 0.7 ML O). Four main peaks appear at masses 29, 32, and 45. The mass-29 peak is clearly due to the CO desorption, which occurs between 32 K and 55 K and peaks at 41 K. Mass 32 presents two peaks, the first one between 28 and 42 K – peaked at 34 K – is due to O_2 desorption while the second one peaking at around 65 K included between 55 K and 75 K is due to the desorption of O_3 detected in the form of O_2^+ fragments, as a result of the O_3 cracking in the head of the QMS. We are certain that this peak comes from O_3 desorption because we also detect the signal at mass 48, which has the same shape, though less intense, of the one at mass 32 in the same temperature range (not shown). Finally, the tiny high-temperature peak also shown in the insert comes from to the CO_2 desorption occurring between 75 and 95 K and peaking at 83 K.

The results of the other set of experiments are very similar to the one just described. In fact, we observe always four peaks (except for the 50 K experiment, where O_2 has already desorbed before starting the TPD), but their intensities change with temperature as shown below. Figure 4 indicates that two molecules are actually formed on the surface, O_3 and CO_2. Moreover, O_2 can also be either formed on the surface via the O + O reaction or come from the beam because of the non-total dissociation of O_2 molecules. Considering all reactants and products and remembering that reactions 2a and 3a can be disregarded, the possible reactions occurring on the surface are listed below:

1a. $CO + O \rightarrow CO_2$
4a. $O + O \rightarrow O_2$
5a. $O + O_2 \rightarrow O_3$
6a. $O + O_3 \rightarrow 2\ O_2$.

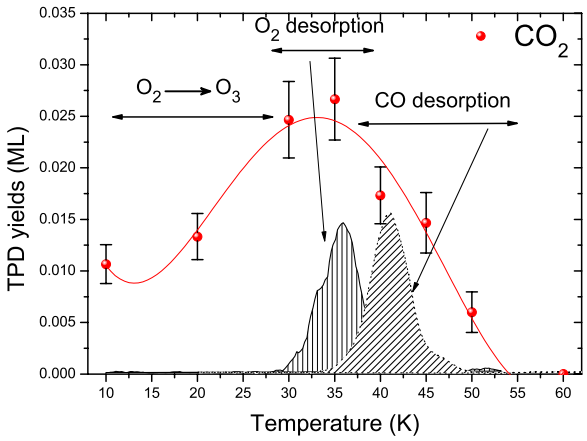

Fig. 5. $^{13}CO_2$ yield as a function of surface temperature during deposition of 0.5 ML of $^{13}CO + O$. Circles represent the integrated area under the TPD curves of mass 45 after a deposition of 0.5 ML of $^{13}CO + O$ on ASW ice held at different temperatures (10 K, 20 K, 30 K, 35 K, 40 K, 45 K, 50 K, 60 K). The solid line is a fit of the area behaviour. The TPD peaks (obtained at $T_{surface}$ = 20 K) added in the figure show when O_2 and ^{13}CO desorb, and this helps interpret the $^{13}CO_2$ yield behaviour with temperature.

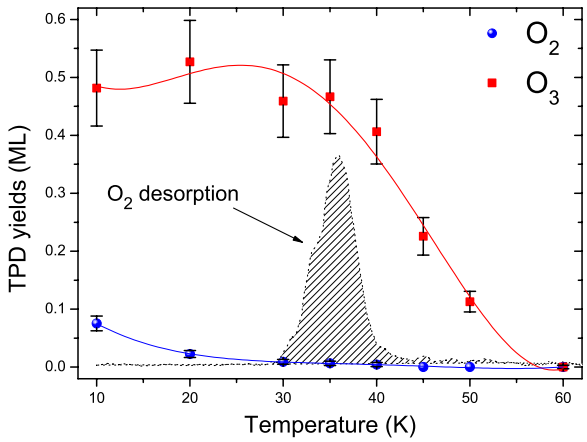

Fig. 6. O_2 and O_3 yields as a function of surface temperature during deposition of 0.5 ML of $^{13}CO + O$. The circles and the squares represent the integrated area under the TPD curves of O_2 and O_3, respectively, after deposition of 0.5 ML of $^{13}CO + O$ on ASW ice held a different temperatures (10 K, 20 K, 30 K, 35 K, 40 K, 45 K, 50 K, 60 K). The solid line is a fit of the area behaviour. The added O_2 TPD (obtained at $T_{surface}$ = 20 K) helps interpret the O_3 yield behaviour with temperature.

Table 1. List of surface reactions with the respective activation barriers.

Reaction	Reactivity observed	Activation barrier
O + O	Yes	<190 K/k_b [a]
O + O_2	Yes	<190 K/k_b [a]
O + O_3	No	>2300 K/k_b [a]
CO + O	Yes	290 K/k_b [b] –780–475 K/k_b [c]
CO + O_2	No	24 000 K/k_b [d]
CO + O_3	No	>3000 K/k_b [c]

References. [(a)] Minissale et al. (2013); [(b)] Roser et al. (2001); [(c)] This work; [(d)] Mallard et al. (1994).

The last three reactions were studied in Minissale et al. (2013). While reactions 4a and 5a seem to be barrier-less (or with a very low activation barrier below 190 K/k_b), reaction 6a does not occur and is likely to have a high activation barrier (see Table 1).

Apparently, reaction 1a is in competition with reactions 4a and 5a. To understand how efficiently the CO + O reaction proceeds and to derive its activation barrier, we performed several experiments at a fixed coverage and by varying the surface temperature. Temperature, in fact, affects both oxygen atom diffusion and the desorption of species and these two processes give us the key to understand our results (Figs. 5 and 6) and consequently the way CO_2 is formed.

As we can see in Fig. 5, the CO_2 signal is already present at 10 K[4], and it reaches a maximum when the surface temperature during exposure is 35 K. Subsequently, for higher temperatures the CO_2 signal decreases and becomes zero at 60 K. This behaviour can be explained by considering three different "temperature zones": below 30 K, between 30 K and 35 K, and higher than 35 K. In the range between 10 K and 30 K, the majority of oxygen atoms are used to produce ozone (Fig. 6) via reaction 4a and 5a, and its production rises with temperature owing to the increase in O diffusion. In this low-temperature zone, only a small amount of oxygen atoms is used to produce CO_2, probably via the Eley-Rideal mechanism, see below. When O_2 starts to desorb (mid-temperature zone, 30–35 K) O atoms have a lower probability of meeting O_2 molecules to form O_3. In fact, we see a decrease in the amount of O_3 desorbed (Fig. 6), while in this range of temperature the probability that an oxygen atom encounters a CO molecule increases (as a consequence of the reduced coverage of O_2). At temperatures higher than 35 K, CO desorption begins and the CO_2 signal begins to drop with same pattern observed for ozone. This suggests that also at high temperatures (45–50 K) molecules and atoms coming from the beam still have a residence time on the surface long enough to react and form appreciable amounts of ozone and CO_2. The shape of the CO_2 and O_3 yields in Figs. 5 and 6 suggest that CO_2 formation is limited by O_2 molecules or, in other words, that reaction 1a is in competition with reactions 4a and 5a. In fact, only when the O_3 signal decreases (and O_2 desorbs) CO_2 formation rises. However, presence of O_2 apart, CO_2 always forms in small amounts, and this very probably indicates the existence of an activation barrier (hereafter E_a) for the reaction CO + O. To evaluate E_a and to understand what surface mechanisms are responsible for CO_2 formation we have developed a model described in the next section.

4. Model

In this section we present the model used to fit our experimental data. It is composed of two sets of differential equations. Reactions 1a, 4a, and 5a can occur through two mechanisms: the Eley-Rideal (ER) and the Langmuir-Hinshelwood (LH) mechanisms. In the ER mechanism one molecule is already adsorbed on the surface and the other comes from the gas phase (i.e., the beam line). In the LH mechanism, both molecules are bound to the surface and by diffusion they can meet each other and react. We consider five species: two are coming exclusively from the beam, O atoms and CO molecules, two are formed only on the surface, O_3 and CO_2, and one, O_2, is coming both from the beam

[4] We know indirectly that CO_2 is formed at deposition temperature, namely, before the TPD. We do not see, in fact, any change in the RAIR spectra of O_3 during the TPD. This means that all O atoms are able to scan the surface, hence to react at deposition temperature (see Minissale et al. 2013, for more details).

and formed on the surface. Below the list of equations governing the CO_2 formation by the ER mechanism follows:

$$O'(t) = 2\tau\,\phi_{O_2off}\,(1 - 2O - O_2) - (1 - \tau)\,\phi_{O_2off}\,O - r_{aER}\,2\tau\phi_{O_2off}CO - r_{aER}\phi_{CO}O \quad (1)$$

$$O_2'(t) = (1 - \tau)\,\phi_{O_2off}\,(1 - O\,(1 - \epsilon)) - 2\tau\,\phi_{O_2off}\,O_2 + 2\tau\,(1 - \epsilon)\,\phi_{O_2off}\,O \quad (2)$$

$$O_3'(t) = (1 - \tau)\,\phi_{O_2off}\,O + 2\tau\,\phi_{O_2off}\,O_2 \quad (3)$$

$$CO'(t) = \phi_{CO} - r_{aER}\,2\tau\,\phi_{O_2off}\,CO - r_{aER}\,\phi_{CO}\,O \quad (4)$$

$$CO_2'(t) = r_{aER}\,2\tau\,\phi_{O_2off}\,CO + r_{aER}\,\phi_{CO}\,O \quad (5)$$

where capital-element symbols express the surface densities (expressed in fraction of ML) of the species, τ is the dissociated fraction of O_2 defined in Sect. 2, $\phi_{O_2off,CO}$ are the fluxes (0.003 cm^{-2} s^{-1}) of O_2 and CO respectively, r_{aER} is the reaction probability of CO + O via ER, and ϵ is the evaporation probability – due to chemical desorption – of O_2 formed on the surface. Simple calculations give that $2\tau\phi_{O_2off}$ and $(1-\tau)\phi_{O_2off}$ are the O and O_2 flux respectively when the discharge is on. Similarly, as for the CO_2 formation by the LH mechanism, we have:

$$O'(t) = -4k\,OO - k\,OO_2 - k\,r_{aLH}\,O\,CO \quad (6)$$

$$O_2'(t) = 2k\,(1 - \epsilon)\,OO - k\,OO_2 - Des_{O_2}\,O_2 \quad (7)$$

$$O_3'(t) = +k\,OO_2 \quad (8)$$

$$CO'(t) = -k\,r_{aLH}\,O\,CO - Des_{CO}\,CO \quad (9)$$

$$CO_2'(t) = +k\,r_{aLH}\,O\,CO \quad (10)$$

where capital element symbols express the surface densities (expressed in ML) of the species, k is the diffusion coefficient of O atoms (the unit of k is ML^{-1} s^{-1}, that can be transformed in the usual unit cm^2 s^{-1} by considering that 1 ML = 10^{15} molecules cm^{-2}), r_{aLH} has the same physical meaning of r_{aER}, but in the case of LH reactions, $Des_{O_2,CO}$ are functions that take into account O_2 and CO desorption. These two functions are expressed through the first-order Polanyi-Wigner equation

$$Des_{O_2(CO)}(T) = \nu\,\exp(-E_{O_2(CO)}/T) \quad (11)$$

where ν is the "attempt frequency" (s^{-1}) for overcoming the barrier to desorption, and $E_{O_2,CO}$ are the activation energies for desorption of O_2 and CO respectively. Our experimental data provide the fraction of ML of each species present on the surface, therefore in this two sets of equation we have six free parameters: $r_{aER,LH}$, $E_{O_2,CO}$, ϵ and k. Actually, four of these parameters have already been studied under very similar experimental conditions (ϵ in Dulieu et al. 2013; k in Minissale et al. 2013, $E_{O_2,CO}$ in Noble et al. 2012), hence by using their measured values we can reduce to two the number of free parameters, namely, r_{aER}, and r_{aLH}; ϵ is equal to zero in the case of a water ice surface while it is 0.5 if the experiments are carried out on graphite. The diffusion coefficient k is a function of the temperature and we describe it using the law $k = k_0(1 + T^3/T_0^3)$, where k_0 is 0.9 and T_0 is 10 K. Finally, the E_{O_2} and E_{CO} desorption barriers are two energy distributions centred at 1310 K/k_b and 1430 K/k_b respectively. In our model, we could have added another couple of parameters, $k_{O_2,CO}$, representing the O_2 and CO diffusion. However, O diffusion is always dominant with respect to O_2 or CO diffusion. The addition of O_2 and CO diffusion would cause a quicker consumption of O atoms, without significant changes of the final amount of species. Introducing two more free parameters would then be of secondary importance for the purpose of this work and it would add more complexity. For these reasons we have chosen to neglect the diffusion of O_2 and CO.

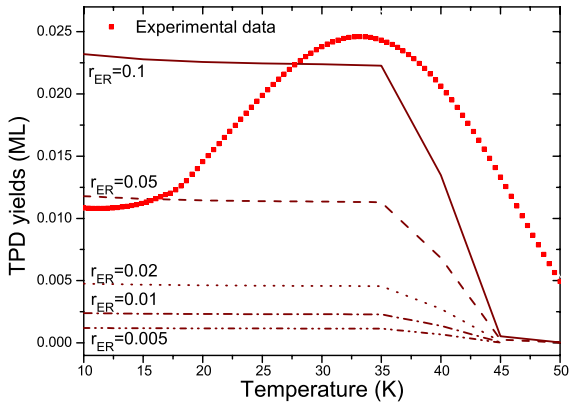

Fig. 7. Model results for CO_2 production on ASW (pure ER). The curves in this figure were obtained by using $r_{LH} = 0$, and different r_{ER} values (ranging from 0.005 to 0.1). The squares are a best fit of the experimental values.

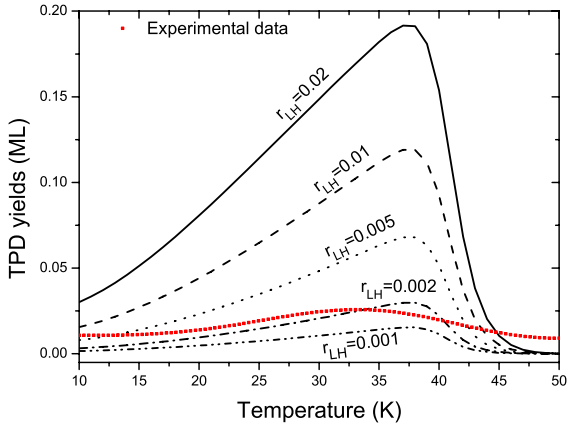

Fig. 8. Model results for CO_2 production on ASW (pure LH). The curves in this figure were obtained by using $r_{ER} = 0$, and different r_{LH} values (ranging from 0.001 to 0.02). The squares are a best fit of the experimental values.

To find the best fit of our experimental values, we have proceeded in this way: we set one of the two parameters to zero and vary the other between 0 and 1. We thus find a value that reproduces the experimental CO_2 yield at 10 K and that at once does not overcome the other experimental CO_2 yields. This value will be an upper limit. In the case of r_{aER}, a value higher than 0.05 returns too much CO_2 (Fig. 7) while in the case of r_{aLH}, the upper limit is around 0.002 (Fig. 8). Then, through the χ^2 test – here we compare the simulated outcome to the experimental values – we have found that the best couple of reaction probabilities is $r_{aER} = 0.021$ and $r_{aLH} = 0.0019$. The model results showing the yields of all species are displayed in Fig. 9. To find acceptable solutions we need concentrate on the CO_2 curve. In fact, the reaction probabilities are the only free parameters of our model and one small variation of them strongly affects the CO_2 curve (r_a appears in each term of the CO_2 equations), that is why the experimental CO_2 yields are the most important constraints in our model. Moreover, the model allows us to distinguish and quantify the contribution to CO_2 formation by either ER or LH mechanism.

In Fig. 10 we show the individual contributions to CO_2 formation by ER or LH mechanism as a function of surface temperature. In Table 2 the CO_2 yield is expressed in monolayers, in units of the normalized amount formed at 10 K, and in fractions

Table 2. Model results showing carbon dioxide yields as a function of surface temperature.

	CO_2 formed by ER			CO_2 formed by LH		
Surface temp. (K)	ML	CO_2 at x K/10 K	% of total	ML	CO_2 at x K/10 K	% of total
10	0.00379	1	57	0.00284	1	43
15	0.00371	0.977474	43	0.00496	1.746934	57
20	0.00365	0.962771	32	0.00823	2.896654	68
25	0.00361	0.951897	22	0.01246	4.386429	78
30	0.00357	0.942215	17	0.01755	6.180850	83
35	0.00353	0.931709	13	0.02342	8.247569	87
40	0.00299	0.789673	10	0.02680	9.436947	90
45	2.8E-4	0.073582	7	0.00367	1.291271	93
50	1.9E-5	0.005049	13	1.2E-4	0.044259	87
55	1.7E-6	4.5E-04	53	1.5E-6	5.4E-04	47
60	1.9E-7	5.2E-05	87	2E-8	1.0E-05	13

Notes. Contributions to CO_2 formation by ER or LH are displayed separately and are expressed in monolayers (ML), normalized yields w.r.t. CO_2 formed at 10 K by the same mechanism, and fractions of the total CO_2 yield.

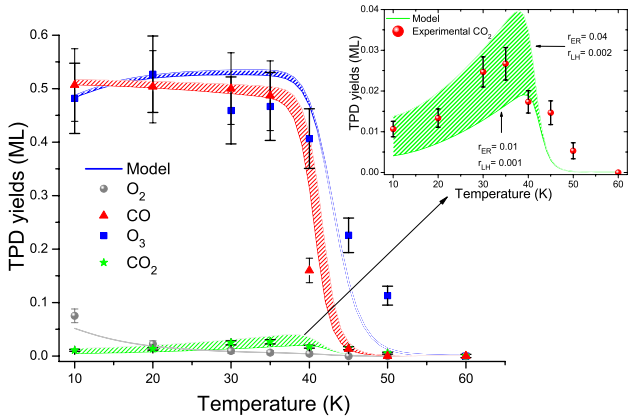

Fig. 9. Model results for all species on ASW. The curves in this figure were obtained by using $r_{LH} = 0.0019 \pm 0.0005$ and $r_{ER} = 0.021 \pm 0.007$. The circles, stars, triangles and squares represent O_2, CO_2, CO, and O_3 experimental results respectively. The *inset* displays a magnified view of the CO_2 yield around its maximum for clarity.

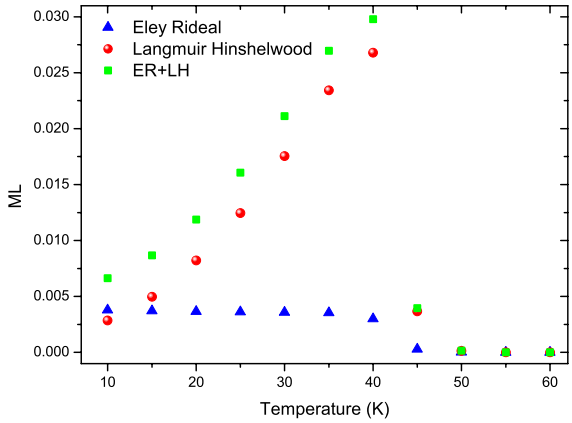

Fig. 10. Model results showing the contribution to CO_2 formation by either ER (triangles) or LH (circles) mechanism. Contributions to CO_2 formation are expressed in monolayers (ML) as a function of surface temperature.

of the total carbon dioxide formed. CO_2 formation via ER mechanism appears to be constant with temperature between 10 and 40 K also because, in theory, this mechanism is temperature independent. At higher surface temperatures, however, ER starts to be inefficient because of the desorption and the decrease of the residence time of species on the surface, thus the CO_2 production efficiency by this mechanism drops off. On the contrary, the LH mechanism depends on the surface temperature and its efficiency increases going from 10 to 40 K owing to the favoured diffusion of atoms. Beyond 40 K, as occurs for the ER case, the probability that O atoms and CO molecules leave the surface is high and the CO_2 yield decreases fast with temperature. The ER and LH contribution to CO_2 formation is approximately equal at low temperatures (below 20 K), while at high temperatures most CO_2 is formed via the LH mechanism. This is not surprising considering the power law dependence on the temperature of the diffusion parameter.

4.1. Evaluation of the CO + O barrier

The two reaction probabilities r_{aER} and r_{aLH} give the probability that the CO + O reaction occurs, thus they have the same physical meaning and can be used to evaluate other physical quantities. By inverting a normalized Arrhenius equation the desorption energy E_a can be calculated as follows:

$$E_a = -k_b\, T_{eff} \log(r_a). \tag{12}$$

Two alternative strategies can be used to evaluate the activation barrier of the reaction; we can derive the reaction barrier E_a either from r_{aER} or r_{aLH}.

4.1.1. ER case

In collision theory, this law is derived by considering gas phase particles described through a Maxwell-Boltzmann (MB) energy distribution and assuming that the interactions between the reactants can occur only via head-on collisions (see Atkins 2006). For ER reactions, the use of Eq. (12) is plausible because the interactions occur between a particle coming from the gas phase (MB distribution) and a particle thermalized with the surface. In this case, somehow similarly to gas phase reactions, the impinging particles either collide and react with one adsorbate or have enough energy to hop on the surface before thermalizing and accommodating in an empty adsorption site. Gas phase molecules coming from the beam-line are at around $T_{gas} = 300 \pm 20$ K/k_b while the target particles adsorbed on the substrate are thermalized with the surface at $T_{solid} = 10{-}60$ K/k_b. The temperature

in Eq. (12) represents the average molecular (atomic) kinetic energy ($\overline{E}$) and in a gas at the thermodynamic equilibrum, $\overline{E}$ is proportional to the thermodynamic temperature. The problem is to know the exact temperature ($T_{\rm eff}$) to insert in Eq. (12). We consider three different cases:

- $T'_{\rm eff} = T_{\rm gas} = 300$ K
- $T''_{\rm eff} = 202 \pm 5$ K.
- $T'''_{\rm eff} = 123 \pm 10$ K.

Evidently, we do not take into account the case $T_{\rm eff} = T_{\rm solid}$, because that means to consider molecules already thermalized with the surface, as in a pure LH process.

In the first case ($T = T_{\rm g} = 300$ K) we obtain a barrier of 1200 K/$k_{\rm b}$. Clearly, in our experiments we cannot consider CO and O as two gases at the same thermodynamic equilibrium so the temperature is likely to be lower than 300 K. This means that $E_{\rm a} = 1200$ K/$k_{\rm b}$ is to be considered only an upper limit of the activation barrier.

The second and third cases are $T_{\rm eff} = 202$, 123 K. This choice is justified by the equation below[5]

$$T_{\rm eff} = \mu\left(\frac{T_{\rm solid}}{m_x} + \frac{T_{\rm gas}}{m_y}\right) \quad (13)$$

where μ is the effective mass of the CO and O system. These temperatures correspond to the velocity of the centre of mass of the system. By substituting their values in Eq. (12), we find a CO + O reaction barrier between $E_{\rm aER} = 780$–475 K/$k_{\rm b}$.

4.1.2. LH case

As stated above, we have also tried to derive the reaction barrier from $r_{\rm aLH}$.

In general, the activation barrier of a process or reaction is the same independently of the mechanism that led to it. As to the LH mechanism, reaction partners adsorbed in the same site collide at the temperature (velocity) of the substrate; the disadvantage with respect to overcoming the barrier in the ER case is the lower energy of the colliding partners, but with the advantage that they will collide ν times per second (usually $\nu = 10^{12-13}$ s^{-1}) instead of only once.

It should be noted that $r_{\rm LH}$ is dependent on the temperature even though we have given a unique value of the reaction probabilities[6]. The temperature dependence of $r_{\rm LH}$ is not as simple as in the Arrhenius case (Eq. (12)). In addition, it cannot be derived from the experimental values because they do not provide enough constraints, hence we give a mean value $\overline{r_{\rm LH}(T)} = 0.0019$ across the whole temperature range investigated (10–60 K). We then try to estimate the reaction barrier by taking into account the two following considerations:

i) although O-atoms diffusion is predominant with respect to that of O_2 and CO, at high temperatures[7] also O_2 and CO diffusion has to be taken into account if a proper evaluation of $r_{\rm LH}$(T) is required.
ii) Non-exponential behaviour of the CO_2 formation rate due to occurrence of tunneling at very low temperatures (Goumans & Andersson 2010, see Fig. 11).

[5] See Appendix A.

[6] This is also true for what concerns the ER mechanism although the variation of $r_{\rm ER}$ with temperature is a minor effect. The uncertainty due to this effect is accounted for by the error bar of the activation barrier.

[7] The onsets of O_2 and CO diffusion take place at 25 K and 30 K, respectively.

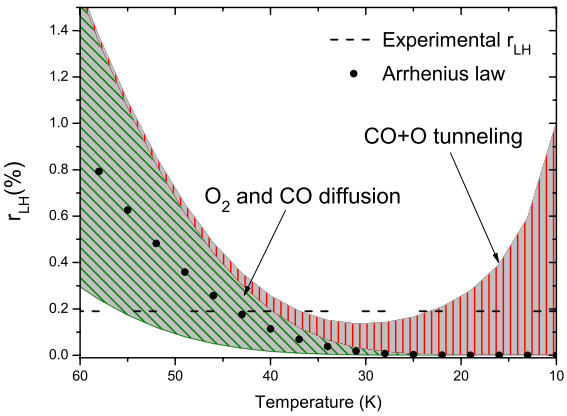

Fig. 11. Temperature dependence of $r_{\rm LH}(T)$ between 10 and 60 K. The two pinstriped regions indicate how a different parametrization of tunneling for CO + O reaction and of O_2 and CO diffusion can change our estimation of $r_{\rm LH}(T)$. The dashed line represents our experimental data. Full circles are an example of a pure Arrhenius behaviour.

These considerations suggest that $r_{\rm LH}(T)$, for $T < 25$ K, is better described by this law

$$r_{\rm LH}(T) = \exp(-E_{\rm a}/k_{\rm b}\,T_{\rm eff}) + r_{\rm tunn}(E_{\rm a}, T) \quad (14)$$

where $r_{\rm tunn}(E_{\rm a}, T)$ (it is ≥ 0) represents the rate of tunneling of the CO + O reaction and it is able to increase the reaction probabilities value at low temperature. By inverting Eq. (14) we have

$$E_{\rm a} = -k_{\rm b}\,T_{\rm eff}\,\log(r_{\rm LH}(T) - r_{\rm tunn}(E_{\rm a}, T)) > -k_{\rm b}\,T_{\rm eff}\,\log(r_{\rm LH}). \quad (15)$$

By putting $T_{\rm eff} = 25$ K in Eq. (15), $r_{\rm LH}(25\ {\rm K}) = 0.0019$ and $r_{\rm tunn}(E_{\rm a}, T) = 0$, thus and we obtain a lower limit for $E_{\rm a}$ of 160 K/$k_{\rm b}$. This value is underestimated for two reasons:

- At 25 K the tunneling term could become to be dominant with respect to the classical one (Arrhenius law), and clearly is not zero.
- $r_{\rm LH}(T)$ is a mean value, and very probably $r_{\rm LH}$(T) presents a minimum around 25 K.

This means that $r_{\rm LH}(25\ {\rm K}) \ll 0.0019$ and $E_{\rm a} \gg 160$ K/$k_{\rm b}$ are consistent with the values obtained for $r_{\rm ER}$.

4.1.3. Conclusions

We have described above how we evaluated the activation barrier of the CO + O reaction. Our model allows us to distinguish which mechanisms (Eley Rideal or Langmuir-Hinshelwood) is at play in different temperature regimes and we are able to give a range of values of the activation barrier of reaction CO + O of 780–475 K/$k_{\rm b}$ (see Table 3). We have to note that these values make sense only in the range of validity of Eq. (12). Our results are summarized in Table 3. Finallly, it should be noted that the range of activation energy barriers given in this work are only apparently inconsistent with the 290 K/$k_{\rm b}$ value of Roser et al. 2001, which can actually be considered one of the diverse cases addressed in the present paper. In fact, they provide an estimation (not a measure) of the barrier by using only the classical LH mechanism (very low $T_{\rm eff}$) (on the other hand the ER mechanism (high $T_{\rm eff}$) with the same barrier would produce more CO_2 than that they observed.). Their estimate can thus be considered a lower limit of the barrier which is included in our study of the LH case (lower limit =160 K/$k_{\rm b}$).

Table 3. Activation barrier.

Methods	LH	ER	ER
Temperature (K)	25	202−123	300
Barrier (K/k_b)	160[a]	780−475 K	1200[b]
(kJ/mol)	1.33[a]	6.48−3.95	9.98[b]
(eV)	0.014[a]	0.067−0.041	0.103[b]

Notes. [(a)] Lower limit. [(b)] Upper limit.

5. Astrophysical conclusions

In this paper we have shown that CO_2 can be formed by the CO + O reaction on cold surfaces, such as amorphous water or oxidized graphite. This reaction is relevant to astrochemistry in that it may explain CO_2 formation on interstellar dust grains by surface reactions and thus justifies its abundance in the solid phase. As mentioned in the introduction, the CO + O reaction competes with the CO + OH reaction (some experimental works have already been conducted by Ioppolo et al. 2013), another non-energetic route to CO_2 formation in space. The CO + OH pathway seems to be facilitated by the low barrier of the reaction, but it has an other type of hindrance. In fact, it requires OH formation first (see Chaabouni et al. 2012; Cuppen et al. 2010, and references therein for details on OH formation in space). In H-rich environments, OH can be formed easily, although it can be very quickly destroyed to form water. These facts suggest that the CO_2(CO + O)/CO_2(CO + OH) ratio strongly depends on three parameters:

- the O/H ratio, very probably the most important parameter;
- the grain temperature: the higher it is the shorter is the H residence time on the grain and thus the probability of OH formation;
- H and O diffusion on the surface: since only the first one is usually considered in models (e.g., Garrod & Pauly 2011), the CO + O contribution is, in our opinion, underestimated.

In conclusion, the CO + O pathway seems to be important in those astrophysical environments where a lack of UV photons forbids the energetic routes leading to CO_2 or in environments with large abundances of atomic oxygen. Although the abundance of O atoms in ISM remains controversial, the detected high abundances of solid CO_2 together with observations of atomic oxygen in the molecular cloud Taurus[8] (Whittet et al. 1998), Sgr B2, and L1689N2[9] (Charnley & Kaufman 2000; Caux et al. 2001), make these environments a good example of where the CO + O reaction can efficiently proceed to form CO_2.

Acknowledgements. The LERMA-LAMAp team in Cergy acknowledges the support of the national PCMI programme founded by CNRS, the Conseil Regional d'Ile de France through SESAME programmes (contract I-07-597R). M.M. acknowledges financial support by LASSIE, a European FP7 ITN Community's Seventh Framework Programme under Grant Agreement No. 238258. We also thank the anonymous referees for the fruitful suggestions. F.D. and M.M. thank Prof. H. T. Diep for fertile discussions.

Appendix A: Equation (13) derivation

The molecules in a gas at ordinary temperatures (i.e. at room temperature) can be considered to be in ceaseless, random motion at high speeds. The average translational kinetic energy for these molecules can be deduced from the Boltzmann distribution. In a gas at the temperature T_{gas}, it can be expressed for one molecule by the following equations,

$$\frac{1}{2}m_x v_x^2 = \frac{1}{2}k_b T_{gas} \Rightarrow v_x^2 = \frac{k_b T_{gas}}{m_x}, \tag{A.1}$$

where v_x and m_x are velocity and mass of the particle x, k_b is the Boltzmann constant.

Our case is just a little bit more complex. We can consider the O + CO system as a two-body problem. We define the reduced mass – the effective inertial mass of the system – as follows

$$m \longrightarrow \mu = \frac{1}{\frac{1}{m_1}+\frac{1}{m_2}} = \frac{m_1 * m_2}{m_1 + m_2}, \tag{A.2}$$

and the relative velocity

$$\boldsymbol{v} = \boldsymbol{v}_1 + \boldsymbol{v}_2,$$

by taking the square of the relative velocity and by doing the average we obtain

$$\left\langle v^2 \right\rangle = \left\langle v_1^2 \right\rangle + \left\langle v_2^2 \right\rangle + \underbrace{\langle 2\boldsymbol{v}_1 \cdot \boldsymbol{v}_2 \rangle}_{=0} = \left\langle v_1^2 \right\rangle + \left\langle v_2^2 \right\rangle,$$

where $\langle 2\boldsymbol{v}_1 \cdot \boldsymbol{v}_2 \rangle = 0$ because of the isotropy of $\boldsymbol{v}_2$.

In the simplest case ($m_1 = m_2$ and all the particles are at T_{gas}) through the equation below

$$\begin{aligned} \frac{1}{2}k_b T_{eff} &= \frac{1}{2}\mu v^2 = \frac{1}{2}k_b \mu \left(\frac{T_{gas}}{m_1} + \frac{T_{gas}}{m_1}\right) \\ &= \frac{1}{2}k_b \mu \frac{2T_{eff}}{m_1} = \frac{1}{2}k_b T_{gas}, \end{aligned} \tag{A.3}$$

it is possible to find the effective temperature of the molecules

$$T_{eff} = T_{gas}. \tag{A.4}$$

In the case (our case) of two different molecules (i.e. CO and O, $m_{CO} \neq m_O$) at different temperatures ($T_{CO} = T_{solid} \neq T_{gas} = T_O$ or $T_O = T_{solid} \neq T_{gas} = T_{CO}$), we will have a reduced mass of

$$\mu = \frac{m_{CO} * m_O}{m_{CO} + m_O} = \frac{29 * 16}{45} = 10.3,$$

then, in the case of CO adsorbed and O arriving from the gas phase,

$$\begin{cases} \frac{1}{2}m_{CO}v_{CO}^2 = \frac{1}{2}k_b T_{solid} \Rightarrow v_{CO}^2 = \frac{k_b T_{solid}}{m_{CO}} \\ \frac{1}{2}m_O v_O^2 = \frac{1}{2}k_b T_{gas} \Rightarrow v_O^2 = \frac{k_b T_{gas}}{m_O}, \end{cases}$$

or, in the case of O adsorbed and CO from gas phase,

$$\begin{cases} \frac{1}{2}m_{CO}v_{CO}^2 = \frac{1}{2}k_b T_{gas} \Rightarrow v_{CO}^2 = \frac{k_b T_{gas}}{m_{CO}} \\ \frac{1}{2}m_O v_O^2 = \frac{1}{2}k_b T_{solid} \Rightarrow v_O^2 = \frac{k_b T_{solid}}{m_O}, \end{cases}$$

and so

$$\frac{1}{2}k_b T''_{eff} = \frac{1}{2}\mu v^2 = \frac{1}{2}k_b \mu \left(\frac{T_{solid}}{m_{CO}} + \frac{T_{gas}}{m_O}\right), \tag{A.5}$$

$$\frac{1}{2}k_b T'''_{eff} = \frac{1}{2}\mu v^2 = \frac{1}{2}k_b \mu \left(\frac{T_{gas}}{m_{CO}} + \frac{T_{solid}}{m_O}\right). \tag{A.6}$$

[8] Taurus is a quiescent dark cloud where CO_2 formation cannot be explained through energetic formation routes.

[9] Sgr B2 is a giant molecular cloud and L1689N where large amounts of atomic oxygen were observed (Lis et al. 2001; Caux et al. 2001).

From these equations, by using $T_{\rm solid} = 25$ K and $T_{\rm gas} = 300$, we obtain

$$T''_{\rm eff} = \mu\left(\frac{T_{\rm solid}}{m_{\rm CO}} + \frac{T_{\rm gas}}{m_{\rm O}}\right) = 202 \text{ K},$$

$$T'''_{\rm eff} = \mu\left(\frac{T_{\rm gas}}{m_{\rm CO}} + \frac{T_{\rm solid}}{m_{\rm O}}\right) = 123 \text{ K}.$$

These two $T_{\rm eff}$ will be used to find a lower and an upper limit for the activation barrier. We have to note that the two reactions $O_{\rm gas} + CO_{\rm solid}$ and $CO_{\rm gas} + O_{\rm solid}$ do not have the same probability of occurring at different temperatures due to a different residence time on the surface and diffusion constant of molecules and atoms and, in the case of $O_{\rm solid}$ strong concurrence with $O + O_2$ reaction. This consideration induces us not to give an exact value of the activation barrier, but just a possible range of values.

References

Aikawa, Y. D., Kamuro, I., Sakon, Y., et al. 2012, A&A, 538, A57
Amiaud, L., Fillion, J.-H., Baouche, S., et al. 2006, J. Chem. Phys., 124, 094702
Atkins, P., & de Paula, J. 2006, Physical Chemistry, Eighth Edition (Oxford)
Caux, E., Ceccarelli, C., Vastel, C., et al. 2001, ESA SP, 460, 223
Chaabouni, H., Minissale, M., Manicó, G., et al. 2012, J. Chem. Phys., 137, 234706
Charnley, S. B., & Kaufman, M. J. 2000, ApJ, 529, L111
Congiu, E., Matar, E., Kristensen, L. E., Dulieu, F., & Lemaire, J. L. 2009, MNRAS, 397, L96
Congiu, E., Chaabouni, H., Laon, C., et al. 2012, J. Chem. Phys., 137, 054713
Cuppen, H. M., Ioppolo, S., Romanzin, C., & Linnartz, H. 2010, Phys. Chem. Chem. Phys., 12, 12077
de Graauw, T., Whittet, D. C. B., Gerakines, P. A., et al. 1996, A&A, 315, L345
d'Hendecourt, L. B., & Jourdain de Muizon, M. 1989, A&A, 223, L5
Dulieu, F., Congiu, E., Noble, J., et al. 2013, Sci. Rep., 3, 1338
Garrod, R. T., & Pauly, T. 2011, ApJ, 735, 15
Gerakines, P. A., Schutte, W. A., & Ehrenfreund, P. 1996, A&A, 312, 289
Gerakines, P. A., Whittet, D. C. B., Ehrenfreund, P., et al. 1999, ApJ, 522, 357
Gibb, E. L., Whittet, D. C. B., Boogert, A. C. A., & Tielens, A. G. G. M. 2004, ApJS, 151, 35
Goumans, T. P. M., Uppal, M. A., & Brown, W. A. 2008, MNRAS, 384, 1158
Hasegawa, T. I., Herbst, E., & Leung, C. M. 1992, ApJS, 82, 167
Herbst, E., & Leung, C. M. 1986, MNRAS, 222, 689
Ioppolo, S., Palumbo, M. E., Baratta, G. A., & Mennella, V. 2009, A&A, 493, 1017
Ioppolo, S., Fedoseev, G., Lamberts, T., Romanzin, C., & Linnartz, H. 2013, RSI, submitted
Jamieson, C. S., Mebel, A. M., & Kaiser, R. I. 2006, ApJS, 163, 184
Knez, C., Boogert, A. C. A., Pontoppidan, K. M., et al. 2005, ApJ, 635, L145
Laffon, C., Lasne, J., Bournel, F., et al. 2010, Phys. Chem. Chem. Phys., 12, 10865
Mallard, W. G., Westley, F., Herron, J. T., Hampson, R. F., & Frizzel, D. H. 2004, NIST Chemical Kinetics Database Version 6.0, National Institute of Standards and Technology, Gaithersbyrg (MD)
Minissale, M., Congiu, E., Baouche, S., et al. 2013, PRL, 111, 053201
Noble, J. A., Dulieu, F., Congiu, E., & Fraser, H. J. 2011, ApJ, 735, 121
Noble, J. A., Congiu, E., Dulieu, F., & Fraser, H. J. 2012, MNRAS, 421, 768
Nummelin, A., Whittet, D. C. B., Gibb, E. L., Gerakines, P. A., & Chiar, J. E. 2001, ApJ, 558, 185
Oba, Y., Watanabe, N., Kouchi, A., Hama, T., & Pirronello, V. 2010, ApJ, 722, 1598
Oliveira, J. M., van Loon, J. Th., Sloan, G. C., et al. 2011, MNRAS, 411, L36
Ootsubo, T., Usui, F., Kawakita, H., et al. 2010, ApJ, 717, L66
Palumbo, M. E., Baratta, G. A., Brucato, J. R., et al. 1998, A&A, 334, 247
Raut, U., & Baragiola, R. 2011, ApJ, 737, L14
Roser, J. E., Vidali, G., Manicó, G., & Pirronello, V. 2001, ApJ, 555, L61
Shimonishi, T., Onaka, T., Kato, D., et al. 2010, A&A, 514, A12
Talbi, D., Chandler, G. S., & Rohl, A. L. 2006, Chem. Phys., 320, 214
Tsuji, T., Yamamura, I., & Sorahana, S. 2011, ApJ, 734, 73
van Dishoeck, E. F., Helmich, F. P., de Graauw, T., et al. 1996, A&A, 315, L349
Whittet, D. C. B., Gerakines, P. A., Tielens, A. G. G. M., et al. 1998, ApJ, 498, L159
Woodruff, D. P., & Delcher, T. A. 1994, Modern Techniques of Surface Science, 2nd edn. (Cambridge: Cambridge University Press)